

# Emergent holon state with a “partially” enlarged electron Fermi surface in the Kondo-Heisenberg model

Jiangfan Wang<sup>1</sup> and Yi-feng Yang<sup>1, 2, 3, \*</sup>

<sup>1</sup>*Beijing National Laboratory for Condensed Matter Physics,*

*Institute of Physics, Chinese Academy of Science, Beijing 100190, China*

<sup>2</sup>*School of Physical Sciences, University of Chinese Academy of Sciences, Beijing 100190, China*

<sup>3</sup>*Songshan Lake Materials Laboratory, Dongguan, Guangdong 523808, China*

(Dated: September 2, 2020)

We develop an efficient algorithm to go beyond the local approximation of the Schwinger boson approach on the Kondo lattice. Its application to the Kondo-Heisenberg model on the square lattice reveals a global phase diagram controlled by a deconfined antiferromagnetic quantum critical point and a Lifshitz transition to a “large” electron Fermi surface, with either an intermediate paramagnetic phase or a single point in between. The intermediate phase is featured with gapless spinon and holon excitations and a “partially” enlarged electron Fermi surface, which is not possible in the local approximation. We discuss their consequences and relevance in real materials.

The interplay of antiferromagnetic (AFM) transition and *f* electron delocalization underlies many exotic properties of the Kondo lattice physics [1, 2]. In particular, the recent discovery of a non-Fermi liquid quantum critical phase in the frustrated Kondo lattice CePdAl has posed an urgent challenge in clarifying the nature of this intermediate state [3], which is in stark contrast with the usual observation of a single quantum critical point (QCP) in many heavy fermion antiferromagnets, such as YbRh<sub>2</sub>Si<sub>2</sub> [4–7], CeRhIn<sub>5</sub> [8, 9], and CeCu<sub>6-x</sub>Au<sub>x</sub> [10–13]. In the latter case, the AFM QCP is often thought to be accompanied with the full delocalization of *f*-electrons into a heavy Fermi liquid (HFL), possibly manifested by an abrupt change of the electron Fermi surface from “small” (no *f* electrons) to “large” (with *f* electrons). In CePdAl, however, the two transitions are detached. The intermediate phase spans over a broad range of the pressure-magnetic field phase diagram and is neither magnetically ordered nor a Fermi liquid. Similar intermediate phase has been observed previously in Ir or Ge-doped YbRh<sub>2</sub>Si<sub>2</sub> [14, 15]. Its origin is unclear, but often attributed to magnetic frustrations, low dimensionality, or large spin/orbital degeneracy [16–19].

The lack of a thorough microscopic understanding lies in the extreme difficulty of simulating the Kondo lattice. The widely used dynamical mean-field theory [20] and its cluster extensions [21, 22] can well capture local or short-range correlations but fail to describe long-range quantum critical fluctuations. Exact lattice simulations often require heavy computational efforts and can only be applied under very special conditions on small lattices [23]. In this regard, the recent development of the large-*N* Schwinger boson approach represented an important advance [24–29]. Compared to the prevalent slave-boson method, the Schwinger boson representation of spins allows for a better treatment of local moment antiferromagnetism and its interplay with Kondo screening. However, its latest implementations on the Kondo lattice have all predicted direct transitions between AFM and HFL,

showing no sign of an intermediate phase [28, 29].

The discrepancy comes from the local approximation adopted in these calculations, which ignores momentum dependence of quasiparticle self-energies in order to reduce the computational efforts [28, 29]. To overcome this issue, we go beyond the local approximation and develop an efficient numerical algorithm to solve the Schwinger boson self-consistent equations with full frequency and momentum-dependent self-energies. This enables us to study the low-energy charge and spin dynamics with both temporal and spatial fluctuations. Our method is then applied to the two-dimensional (2D) Kondo-Heisenberg model on the square lattice and finds in certain parameter range an emergent intermediate state featured with gapless spinon and holon excitations, as well as a “partially” enlarged electron Fermi surface due to the generalized Luttinger sum rule [30, 31], which is forbidden in the local approximation. The phase diagram and finite temperature properties are controlled by the interplay of a deconfined AFM QCP and a Lifshitz transition of the Fermi surface, which merge together into a single transition for large spin size. We discuss their consequences and relevance in real heavy fermion systems.

We start with the following Hamiltonian:

$$H = t \sum_{\langle ij \rangle} c_{i\alpha a}^\dagger c_{j\alpha a} + J_K \sum_i \mathbf{S}_i \cdot \mathbf{s}_i + J_H \sum_{\langle ij \rangle} \mathbf{S}_i \cdot \mathbf{S}_j, \quad (1)$$

where  $c_{i\alpha a}^\dagger$  creates a conduction electron of spin  $\alpha$  and channel (orbital)  $a = 1, 2, \dots, K$  on site  $i$ ,  $\mathbf{s}_i$  is its spin operator, and  $\mathbf{S}_i$  denotes the local spin. The Schwinger boson approach enlarges the SU(2) spin group to the symplectic group Sp(*N*) such that  $\mathbf{S}_i \rightarrow S_i^{\alpha\beta} = b_{i\alpha}^\dagger b_{i\beta} - \tilde{\alpha} \tilde{\beta} b_{i,-\beta}^\dagger b_{i,-\alpha}$ , where  $b_{i\alpha}$  represents the Schwinger boson (spinon),  $\alpha = \pm 1, \dots, \pm N/2$ , and  $\tilde{\alpha} = \text{sgn}(\alpha)$  [32]. A local constraint is then imposed to reduce the enlarged Hilbert space to physical subspace,  $n_{b,i} \equiv \sum_\alpha b_{i\alpha}^\dagger b_{i\alpha} = 2S$ , which may be implemented by introducing the Lagrange multiplier,  $\sum_i \lambda_i (n_{b,i} - 2S)$ . A biquadratic ex-

change term,  $-\zeta J_H \sum_{\langle ij \rangle} (\mathbf{S}_i \cdot \mathbf{S}_j)^2$ , is often included to avoid artificial first-order transitions at large  $N$ , which can be absorbed into the quadratic term under SU(2) symmetry [33]. Depending on the ratio of  $2S/K$ , there exist three distinct regions, where the local spins are either underscreened ( $2S/K > 1$ ), overscreened ( $2S/K < 1$ ), or exactly-screened ( $2S/K = 1$ ) [34]. We focus on the exactly-screened case. The Kondo and Heisenberg terms can be factorized using two auxiliary fields:

$$\begin{aligned} \frac{J_K}{N} S_i^{\alpha\beta} c_{i\beta a}^\dagger c_{i\alpha a} &\rightarrow \frac{1}{\sqrt{N}} b_{i\alpha}^\dagger c_{i\alpha a} \chi_{ia} + h.c. + \frac{|\chi_{ia}|^2}{J_K}, \\ \frac{J_H}{N} S_i^{\alpha\beta} S_j^{\beta\alpha} &\rightarrow \tilde{a} b_{j,-\alpha}^\dagger b_{i,\alpha}^\dagger \Delta_{ij} + h.c. + \frac{N|\Delta_{ij}|^2}{J_H}, \end{aligned} \quad (2)$$

where  $\Delta_{ij}$  denotes the spin-singlet valence bond on adjacent sites and  $\chi_{ia}^\dagger$  can be viewed as a composite fermion of the Kondo state formed by a conduction hole and a spinon.  $\chi_{ia}^\dagger$  is also called the holon field since it carries a positive electric charge and has no spin.

To proceed, we assume the mean-field variables  $\lambda_i = \lambda$  and  $\Delta_{i,i+\hat{x}} = \Delta_{i,i+\hat{y}} = \Delta$ . The former replaces the local constraint  $n_{b,i} = 2S$  by the average spinon occupation and the latter describes a candidate spin liquid energetically favored in the Heisenberg model [35]. The rotational symmetry is preserved under combined operation of lattice rotation and gauge transformation [36]. In the large- $N$  limit, the spinon and holon self-energies are [37]:

$$\begin{aligned} \Sigma_b(\mathbf{p}, i\nu_n) &= -\frac{\kappa}{\beta\mathcal{V}} \sum_{\mathbf{k}\mathbf{m}} g_c(\mathbf{p} - \mathbf{k}, i\nu_n - i\omega_m) G_\chi(\mathbf{k}, i\omega_m), \\ \Sigma_\chi(\mathbf{p}, i\omega_m) &= \frac{1}{\beta\mathcal{V}} \sum_{\mathbf{k}\mathbf{n}} g_c(\mathbf{k} - \mathbf{p}, i\nu_n - i\omega_m) G_b(\mathbf{k}, i\nu_n), \end{aligned} \quad (3)$$

where  $g_c$  is the bare Green's function of conduction electrons,  $G_b$  and  $G_\chi$  are the full Green's functions of spinons and holons to be self-consistently determined by their self-energies,  $\omega_m$  ( $\nu_n$ ) are the fermionic (bosonic) Matsubara frequencies,  $\beta$  is the inverse temperature, and  $\mathcal{V}$  is the total number of lattice sites. The parameter  $\kappa \equiv 2S/N = K/N$  controls the effective strength of quantum fluctuations. The self-energy of conduction electrons is absent in the large- $N$  limit, thus preventing proper treatment of electric transport. In previous calculations [27–29], a local approximation was adopted to reduce the computational efforts by ignoring the momentum dependence of the self-energies. This is equivalent to assign independent electron baths for each local spin as illustrated in Fig. 1(a). Under this approximation, only direct phase transitions are allowed as shown in the inset of Fig. 1(b). To overcome this issue, we notice that the momentum convolution can be turned into a simple multiplication in the coordinate space,  $\Sigma_{b/\chi}(\mathbf{r}) \sim g_c(\mathbf{r}) G_{\chi/b}(\mathbf{r})$ , which motivates us to develop an efficient algorithm based on the fast Fourier transform (FFT) and solve the above equations in coordinate space without approximation [37].

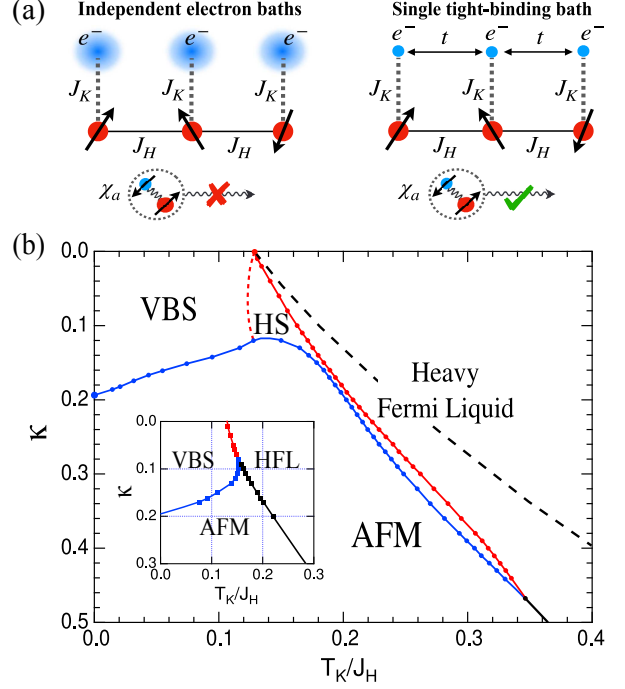


FIG. 1: (a) Illustration of the holon propagation with independent electron baths (local approximation) or a single shared bath (this work). (b) Theoretical phase diagram for the 2D Kondo-Heisenberg model on the square lattice in terms of  $\kappa$  and  $T_K/J_H$ , showing four major phases: the valence bond solid (VBS) state, the local moment AFM phase, the heavy Fermi liquid (HFL) and the intermediate holon state (HS). The AFM and HFL phase boundaries merge together for  $\kappa \geq 0.47$ . The dashed line inside the HFL separates two regions with finite short-range magnetic correlations ( $\Delta \neq 0$ ) or a local Fermi liquid ( $\Delta = 0$ ). The inset compares the phase diagram derived based on the local approximation, showing direct transitions between all three phases.

Figure 1(b) plots the resulting zero-temperature phase diagram on the  $\kappa$  and  $T_K/J_H$  plane, where  $T_K = D e^{-2D/J_K}$  is the single ion Kondo temperature and  $D$  is the half bandwidth of conduction electrons.  $T_K/J_H$  is also called the Doniach ratio. The phase diagram contains four regions: the AFM Néel order, the valence bond solid (VBS) state with a small electron Fermi surface, the HFL with a large electron Fermi surface, and the intermediate holon state (HS) with gapless spinon and holon excitations. The AFM phase boundary is determined by the divergence of the staggered magnetic susceptibility. The holon bands are empty in the VBS state, partially occupied in the HS region, and fully occupied in the HFL. The AFM and HFL transitions merge together to form a single QCP beyond  $\kappa \approx 0.47$ . Inside the HFL, short-range magnetic correlations may vanish ( $\Delta = 0$ ) at large  $T_K/J_H$  and we enter a local Fermi liquid with independently screened spins.

The VBS, AFM and HFL phases are already present in the local approximation and can be largely understood

by two limits. In the Heisenberg limit ( $J_K = 0$ ), the spins are decoupled from conduction electrons. The VBS state is developed once gauge fluctuations are included at finite  $N$  and, depending on the size of the spin  $S$ , may break the lattice symmetry [38, 39]. The AFM phase is associated with spinon condensation at  $\pm(\pi/2, \pi/2)$ , half of the AFM ordering wave vector. The transition between them marks a deconfined QCP with divergent spinon confinement length [40]. The critical  $\kappa_c \approx 0.195$  can be derived analytically from the constraint conditions [37]. We can reproduce the scaling of the staggered susceptibility  $\chi_{st} \propto T^2 e^{4\pi\rho_s/T}$  ( $\rho_s$ : the spin stiffness) in the renormalized classical regime above the Néel order and  $\chi_{st} \propto T^{-2+\eta}$  ( $\eta$ : the anomalous dimension) in the quantum critical regime [41, 42]. The QCP was originally thought to be of the 3D classical Heisenberg universality class with  $\eta \approx 0.033$  [43]. However, our calculations yield a much larger  $\eta$  approaching unity at  $\kappa_c$ , in better agreement with the later prediction by large- $N$  calculations of the  $CP^{N-1}$  model ( $\eta = 1 - 32/\pi^2 N$ ) [44, 45] and direct Monte Carlo simulations of the hedgehog suppressed  $O(3)$  sigma model and the noncompact  $CP^1$  model ( $\eta \approx 0.6$  or  $0.7$ ) [46]. In the limit of  $\kappa \rightarrow 0$ , both spinons and holons are localized and the lattice physics is reduced to a collection of decoupled spins ( $\Delta = 0$ ) undergoing independent Kondo screening beyond a critical  $T_K/J_H$ . For finite  $\kappa$ , the local approximation predicts direct transitions between three states, supporting the celebrated local quantum criticality [47].

By contrast, our calculations with momentum dependent quasiparticle self-energies reveal an intermediate phase (HS) with gapless spinon and holon excitations for  $\kappa < 0.47$ . Importantly, at finite  $J_K$ , we obtain the correct zero temperature AFM instability, in conformity with the Mermin-Wagner theorem [48], while the local approximation predicted falsely a transition at finite temperature [29]. Lattice propagations are crucial for both results, which yield a dispersive holon band and a holon Fermi surface determined by the poles of  $G_\chi$  at the Fermi energy or, equivalently, the effective Kondo coupling,  $J_K^*(\mathbf{p}) \equiv [J_K^{-1} + \text{Re}\Sigma_\chi(\mathbf{p}, 0)]^{-1}$ . Physically, the momentum dependence of  $J_K^*(\mathbf{p})$  implies an unusual nonlocal and cooperative scattering process described by  $J_K^*(\mathbf{r}_j - \mathbf{r}_i) c_{ja\beta}^\dagger b_{j\beta} b_{i\alpha}^\dagger c_{ia\alpha}$ , in which a conduction hole and a spinon form a spinless quasi-bound state (holon) at  $\mathbf{r}_i$ , propagate to another site  $\mathbf{r}_j$ , and then unbound themselves. Such nonlocal and cooperative Kondo effect mediated by fractional quasiparticles is conceptually different from the partial Kondo screening proposed earlier for frustrated Kondo lattice, where local spins and electrons are both intact [18, 23].

The holon Fermi volume,  $V_{\text{FS}}^\chi = \mathcal{V}^{-1} \sum_{\mathbf{p}} \theta(-J_K^*(\mathbf{p}))$ , is gauge invariant and evolves continuously in the intermediate state, as plotted in Fig. 2(b) for  $\kappa = 0.1$ . It satisfies the generalized Luttinger sum rule,  $NV_{\text{FS}}^c - V_{\text{FS}}^\chi = n_c$ , where  $V_{\text{FS}}^c$  is the Fermi volume of conduction electrons

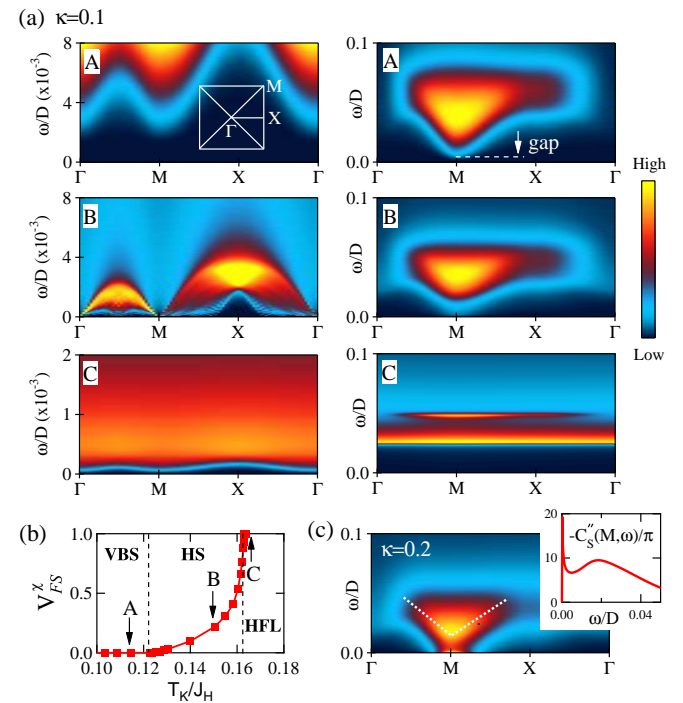


FIG. 2: (a) Holon (left panel) and spin (right panel) excitation spectra along the high symmetry line of the Brillouin zone (inset) at  $\kappa = 0.1$  for  $T_K/J_H = 0.115, 0.15$  and  $0.164$  (from top to bottom) with different ground states as marked in (b). The color represents the intensity of the spectral functions  $-C''_{n_\chi}(\mathbf{k}, \omega)/\pi$  and  $-C''_S(\mathbf{k}, \omega)/\pi$ , respectively. (b) Evolution of the holon Fermi volume,  $V_{\text{FS}}^\chi$ , as a function of  $T_K/J_H$  at  $\kappa = 0.1$ . (c) The spin spectral function at  $\kappa = 0.2$  and  $T_K/J_H = 0.2$  at a small but finite  $T$  right above the AFM ground state. The spectra are highly damped and the white dashed lines are a guide to the eye. The inset shows  $-C''_S(\mathbf{k}, \omega)/\pi$  at  $M$  point as a function of  $\omega/D$ .

and  $n_c$  is the electron number per channel (orbital) [30]. The sum rule reflects the electric charge conservation associated with the  $U(1)$  gauge symmetry:  $\chi_{ia} \rightarrow \chi_{ia} e^{i\phi_a}$ ,  $c_{iaa} \rightarrow c_{iaa} e^{-i\phi_a}$ . As a result, the Fermi surface of conduction electrons is “small” ( $NV_{\text{FS}}^c = n_c$ ) in the VBS phase, “large” ( $NV_{\text{FS}}^c = n_c + 1$ ) in the HFL, but “partially” enlarged in between. For the local approximation, because  $G_\chi = (-J_K^{-1} - \Sigma_\chi)^{-1}$ , the holons have no dispersion and their Fermi volume is either zero or unity, thus preventing a partially enlarged electron Fermi surface. We note that the HS phase is different from the FL\* discussed in Ref. [49]. The latter is characterized by decoupled spinons and a small electron Fermi surface. The existence of a partially enlarged Fermi surface may be best examined by quantum oscillation experiment but could also have an effect on Hall measurement [50].

More detailed information on the low-energy spin and charge excitations in the intermediate state can be extracted from the holon density-density correlation function  $C_{n_\chi} = -\frac{1}{K} \langle n_\chi(\mathbf{r}_i, \tau) n_\chi(\mathbf{r}_j, \tau') \rangle_c$ , where  $n_\chi(\mathbf{r}_i, \tau) =$

$\sum_a |\chi_{ia}(\tau)|^2$ , and the dynamic spin structure factor  $C_S = -\frac{1}{N} \langle S_i^z(\tau) S_j^z(\tau') \rangle_c$  with  $S_i^z = \sum_\alpha \tilde{a} b_{i\alpha}^\dagger b_{i\alpha}$ . The subscript “ $c$ ” denotes that only connected diagrams are considered. Figure 2(a) plots their imaginary parts in the energy-momentum space at  $\kappa = 0.1$  for specially chosen values of  $T_K/J_H$ . We find that both excitations are gapped in the VBS (panel A) and HFL (panel C) phases. In the intermediate state (panel B), the holons become gapless around  $\Gamma$  and  $M$ , corresponding to particle-hole pairs from same or different parts of the holon Fermi surface. With increasing  $T_K/J_H$ , the holon bands ( $D_\chi$ ) become increasingly narrow, implying a heavy effective mass as large as  $m_\chi^*/m_e \propto D/D_\chi \approx 10^4$  on the verge of the HFL boundary. Across the boundary, the holon Fermi surface undergoes a Lifshitz transition and vanishes in the HFL state. Accordingly, conduction electrons achieve a large Fermi surface following the Luttinger sum rule. The spin excitation spectra in the intermediate state are also gapless but highly damped. For the square lattice model in the Heisenberg limit, the spectra are instead sharply defined but gapped outside of the AFM phase. Here the coupling with holons smears out the gap and results in gapless but damped spin excitations. For comparison, Fig. 2(c) shows the results for  $\kappa = 0.2$  at small but finite temperature above the AFM ground state. We find a sharp peak near zero energy as the precursor of spinon condensation. This distinguishes the spinon dynamics near the AFM QCP and inside the intermediate phase, which will have an effect on the finite temperature properties with important implications for CePdAl. At  $\kappa = 0.48$ , the AFM QCP marks a direct transition to the HFL and is featured with both critical spinons and heavy holons.

Thus, the overall phase diagram for  $\kappa > 0.1$  is largely controlled by the interplay of a deconfined AFM QCP and a Lifshitz transition to the large electron Fermi surface. At finite temperature, one may further expect a crossover line connecting to the renormalized classical regime in the Heisenberg limit above the AFM order, and a delocalization line associated with the Lifshitz transition. In between, irrespective of an intermediate state or a single QCP at zero temperature, there always exists a paramagnetic region with short-lived spinon and holon excitations and a “partially” enlarged electron Fermi surface. This provides a candidate microscopic interpretation of the two fluid model with coexisting spin liquid and heavy quasiparticles [51, 52]. The partially enlarged electron Fermi surface evolves with temperature, supported lately by angle-resolved photoemission spectroscopy (ARPES) [53] and ultrafast optical pump-probe spectroscopy [54] in CeCoIn<sub>5</sub>. The fact that it varies continuously and is nearly “large” in the vicinity of the QCP for large  $\kappa$  might help resolve the recent controversy in YbRh<sub>2</sub>Si<sub>2</sub>, where, contrary to usual expectation, ARPES reported a “large” Fermi surface above the AFM transition (70 mK) [55]. Deep on the AFM side, band bending

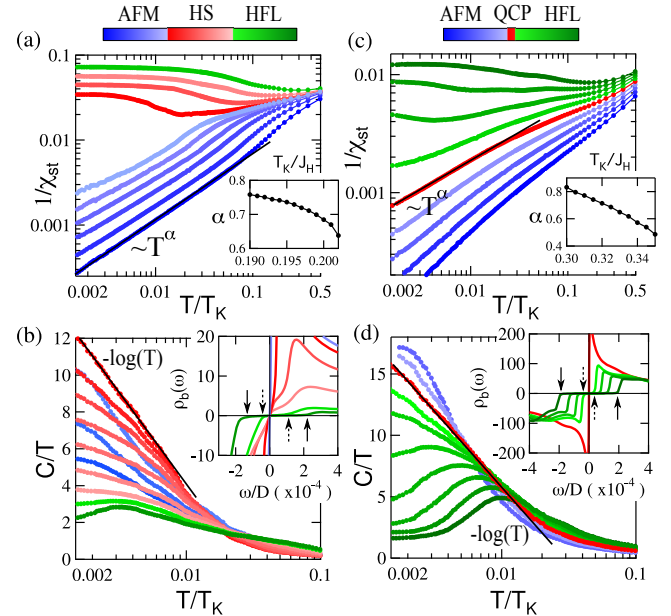


FIG. 3: Temperature dependence of (a) the inverse staggered susceptibility and (b) the specific heat coefficient at  $\kappa = 0.2$  for different values of  $T_K/J_H$ . The colors distinguish the AFM (blue), HS (red), and HFL (green) regions. The inset of (a) shows the power-law exponent  $\alpha$  as a function of  $T_K/J_H$  on the AFM side, and that of (b) compares the low temperature spinon density of states in the HS and HFL regions. The arrows mark the gap edges. (c) and (d) are similar plots at  $\kappa = 0.48$ , where the red color denotes the QCP.

has also been observed in paramagnetic CeRhIn<sub>5</sub> [56].

Some of the physical properties in the intermediate region can be approximately captured by the large- $N$  limit. Figure 3 plots the calculated staggered magnetic susceptibility  $\chi_{st}$  and specific heat coefficient  $C/T$  at  $\kappa = 0.2$  and 0.48. In both cases, we see  $\chi_{st} \sim T^{-\alpha}$  on the AFM side and  $C/T \sim -\ln T$  at the AFM QCP, typical of non-Fermi liquid. The exponent  $\alpha$  varies monotonically with  $T_K/J_H$  and drops rapidly near the AFM QCP (roughly 0.5 at  $\kappa = 0.48$ ). Its value is much smaller than that of the Heisenberg model, reflecting the presence of additional holon excitations. Its nonuniversality seems consistent with experimental observations, where  $\alpha$  varies from 1/3 in UCu<sub>5-x</sub>Pd<sub>x</sub> [57] to 0.51 in Ce(Ru<sub>1-x</sub>Fe<sub>x</sub>)<sub>2</sub>Ge<sub>2</sub> [58] to 0.75 in CeCu<sub>5.9</sub>Au<sub>0.1</sub> [11], apart from other possible reasons. Inside the HFL,  $C/T$  shows a broad maximum at finite temperature. Their difference may be understood from the insets of Figs. 3(b) and 3(d), where the spinon density of states is singular at the AFM QCP but gapped in the HFL. In the intermediate state,  $C/T$  keeps growing with lowering temperature but shows no universal scaling, indicating that the spinon and holon dynamics are not critical away from the phase boundaries for the square lattice model.

It remains to be seen how electric transport properties might be affected once the electron self-energy is included

at finite  $N$ . A linear-in- $T$  resistivity has been proposed for critical holons [28] or due to spinon scattering with vanishing holon velocity at the Fermi energy [31]. This might be true near the AFM QCP, but must not be extended to the whole intermediate region where spinon and holon dynamics are not always critical, even for frustrated Kondo lattices. As a matter of fact, the linear-in- $T$  resistivity was only observed over a very narrow region of the intermediate phase in CePdAl, either near the AFM QCP or where the two transitions are close [3]. Its appearance is most probably associated with the distorted Kagome structure, which might not only promote the holon state but also allow for unusual spinon dynamics away from the AFM QCP within certain parameter region. Schwinger boson calculations on the Kagome lattice model require substantially more auxiliary fields and will be left for future work.

The intermediate phase has also been observed in several other compounds including  $\text{YbRh}_2\text{Si}_2$  with Ir or Ge doping [14, 15] and  $\text{YbAgGe}$  under magnetic field [59]. These compounds adopt different crystal structures, suggesting that it is not a phenomenon solely for frustrated Kondo lattices. Large spin/orbital degeneracy and low dimensionality may also introduce strong quantum fluctuations [60], giving rise to the holon state at small  $\kappa$  in our calculations. Of course, details of the phase diagram may be altered by finite  $N$  corrections including gauge fluctuations. Nevertheless, our approach allows for the possibility of the intermediate state, which is an advance beyond the local approximation. More elaborate studies along this line may lead to a better understanding of the Kondo lattice physics.

This work was supported by the National Key R&D Program of China (Grant No. 2017YFA0303103), the National Natural Science Foundation of China (Grants No. 11774401, No. 11974397), and the Strategic Priority Research Program of the Chinese Academy of Sciences (Grant No. XDB33010100).

---

\* yifeng@iphy.ac.cn

[1] Q. Si and F. Steglich, *Science* **329**, 1161 (2010).  
[2] Y.-F. Yang, D. Pines, and G. Lonzarich, *Proc. Natl. Acad. Sci. U.S.A.* **114**, 6250 (2017).  
[3] H. Zhao, J. Zhang, M. Lyu, S. Bachus, Y. Tokiwa, P. Gegenwart, S. Zhang, J. Cheng, Y.-F. Yang, G. Chen, Y. Isikawa, Q. Si, F. Steglich, and P. Sun, *Nat. Phys.* **15**, 1261 (2019).  
[4] J. Custers, P. Gegenwart, H. Wilhelm, K. Neumaier, Y. Tokiwa, O. Trovarelli, C. Geibel, F. Steglich, C. Pépin, and P. Coleman, *Nature* **424**, 524 (2003).  
[5] S. Paschen, T. Lühmann, S. Wirth, P. Gegenwart, O. Trovarelli, C. Geibel, F. Steglich, P. Coleman, and Q. Si, *Nature* **432**, 881 (2004).  
[6] S. Friedemann, N. Oeschler, S. Wirth, C. Krellner, C. Geibel, F. Steglich, S. Paschen, S. Kirchner, and Q. Si, *Proc. Natl. Acad. Sci. U.S.A.* **107**, 14547 (2010).  
[7] L. Prochaska, X. Li, D. C. MacFarland, A. M. Andrews, M. Bonta, E. F. Bianco, S. Yazdi, W. Schrenk, H. Detz, A. Limbeck, Q. Si, E. Ringe, G. Strasser, J. Kono, and S. Paschen, *Science* **367**, 285 (2020).  
[8] T. Park, F. Ronning, H. Q. Yuan, M. B. Salamon, R. Movshovich, J. L. Sarrao, and J. D. Thompson, *Nature* **440**, 65 (2006).  
[9] H. Shishido, R. Settai, H. Harima, and Y. Ōnuki, *J. Phys. Soc. Jpn.* **74**, 1103 (2005).  
[10] H. v. Löhneysen, S. Mock, A. Neubert, T. Pietrus, A. Rosch, A. Schröder, O. Stockert, and U. Tutsch, *J. Magn. Magn. Mater.* **177**, 12 (1998).  
[11] A. Schröder, G. Aeppli, R. Coldea, M. Adams, O. Stockert, H. v. Löhneysen, E. Bucher, R. Ramazashvili, and P. Coleman, *Nature* **407**, 351 (2000).  
[12] M. Klein, A. Nuber, F. Reinert, J. Kroha, O. Stockert, and H. v. Löhneysen, *Phys. Rev. Lett.* **101**, 266404 (2008).  
[13] M. Klein, J. Kroha, H. v. Löhneysen, O. Stockert, and F. Reinert, *Phys. Rev. B* **79**, 075111 (2009).  
[14] S. Friedemann, T. Westerkamp, M. Brando, N. Oeschler, S. Wirth, P. Gegenwart, C. Krellner, C. Geibel, and F. Steglich, *Nat. Phys.* **5**, 465 (2009).  
[15] J. Custers, P. Gegenwart, C. Geibel, F. Steglich, P. Coleman, and S. Paschen, *Phys. Rev. Lett.* **104**, 186402 (2010).  
[16] Q. Si, *Physica B Condens. Matter* **378**, 23 (2006).  
[17] P. Coleman and A. H. Nevidomskyy, *J. Low. Temp. Phys.* **161**, 182 (2010).  
[18] J. H. Pixley, R. Yu, and Q. Si, *Phys. Rev. Lett.* **113**, 176402 (2014).  
[19] T. Tomita, K. Kuga, Y. Uwatoko, P. Coleman, and S. Nakatsuji, *Science* **349**, 506 (2015).  
[20] A. Georges, G. Kotliar, W. Krauth, and M. J. Rozenberg, *Rev. Mod. Phys.* **68**, 13 (1996).  
[21] L. C. Martin and F. F. Assaad, *Phys. Rev. Lett.* **101**, 066404 (2008).  
[22] D. Tanasković, K. Haule, G. Kotliar, and V. Dobrosavljević, *Phys. Rev. B* **84**, 115105 (2011).  
[23] T. Sato, F. F. Assaad, and T. Grover, *Phys. Rev. Lett.* **120**, 107201 (2018).  
[24] J. Rech, P. Coleman, G. Zarand, and O. Parcollet, *Phys. Rev. Lett.* **96**, 016601 (2006).  
[25] E. Lebanon, J. Rech, P. Coleman, and O. Parcollet, *Phys. Rev. Lett.* **97**, 106604 (2006).  
[26] E. Lebanon and P. Coleman, *Phys. Rev. B* **76**, 085117 (2007).  
[27] Y. Komijani and P. Coleman, *Phys. Rev. Lett.* **120**, 157206 (2018).  
[28] Y. Komijani and P. Coleman, *Phys. Rev. Lett.* **122**, 217001 (2019).  
[29] J. Wang, Y.-Y. Chang, C.-Y. Mou, S. Kirchner, and C.-H. Chung, arXiv: 1901.10411 (2019).  
[30] P. Coleman, I. Paul, and J. Rech, *Phys. Rev. B* **72**, 094430 (2005).  
[31] C. Pépin, *Phys. Rev. Lett.* **94**, 066402 (2005).  
[32] R. Flint and P. Coleman, *Phys. Rev. B* **79**, 014424 (2009).  
[33] T. N. D. Silva, M. Ma, and F.-C. Zhang, *Phys. Rev. B* **66**, 104417 (2002). We have chosen a constant  $\zeta \approx 0.33$  to remove possible first-order transitions for all values of  $\kappa$  in this work. A smaller  $\zeta \approx 0.001$  was used for the 1D ferromagnetic Kondo-Heisenberg model [27].  
[34] O. Parcollet and A. Georges, *Phys. Rev. Lett.* **79**, 4665

(1997).

[35] N. Read and S. Sachdev, Phys. Rev. Lett. **66**, 1773 (1991).

[36] X.-G. Wen, Phys. Rev. B **65**, 165113 (2002).

[37] See Supplemental Material for more theoretical and numerical details.

[38] N. Read and S. Sachdev, Phys. Rev. Lett. **62**, 1694 (1989).

[39] N. Read and S. Sachdev, Phys. Rev. B **42**, 4568 (1990).

[40] T. Senthil, A. Vishwanath, L. Balents, S. Sachdev, and M. P. A. Fisher, Science **303**, 1490 (2004).

[41] S. Chakravarty, B. I. Halperin, and D. R. Nelson, Phys. Rev. B **39**, 2344 (1989).

[42] A. V. Chubukov, S. Sachdev, and J. Ye, Phys. Rev. B **49**, 11919 (1994).

[43] C. Holm and W. Janke, Phys. Rev. B **48**, 936 (1993).

[44] R. K. Kaul and S. Sachdev, Phys. Rev. B **77**, 155105 (2008).

[45] R. K. Kaul and A. W. Sandvik, Phys. Rev. Lett. **108**, 137201 (2012).

[46] O. I. Motrunich and A. Vishwanath, Phys. Rev. B **70**, 075104 (2004).

[47] Q. Si, S. Rabello, K. Ingersent, and J. L. Smith, Nature **413**, 804 (2001).

[48] N. D. Mermin and H. Wagner, Phys. Rev. Lett. **17**, 1133 (1966).

[49] T. Senthil, S. Sachdev, and M. Vojta, Phys. Rev. Lett. **90**, 216403 (2003).

[50] J. Zhang, H. Zhao, M. Lv, S. Hu, Y. Isikawa, Y.-F. Yang, Q. Si, F. Steglich, and P. Sun, Phys. Rev. B **97**, 235117 (2018).

[51] Y.-F. Yang and D. Pines, Proc. Natl. Acad. Sci. U.S.A. **109**, E3060 (2012).

[52] Y.-F. Yang, Rep. Prog. Phys. **79**, 074501 (2016).

[53] Q. Y. Chen, D. F. Xu, X. H. Niu, J. Jiang, R. Peng, H. C. Xu, C. H. P. Wen, Z. F. Ding, K. Huang, L. Shu, Y. J. Zhang, H. Lee, V. N. Strocov, M. Shi, F. Bisti, T. Schmitt, Y. B. Huang, P. Dudin, X. C. Lai, S. Kirchner, H. Q. Yuan, and D. L. Feng, Phys. Rev. B **96**, 045107 (2017).

[54] Y. P. Liu, Y. J. Zhang, J. J. Dong, H. Lee, Z. X. Wei, W. L. Zhang, C. Y. Chen, H. Q. Yuan, Y.-F. Yang, and J. Qi, Phys. Rev. Lett. **124**, 057404 (2020).

[55] K. Kummer, S. Patil, A. Chikina, M. Güttler, M. Höppner, A. Generalov, S. Danzenbächer, S. Seiro, A. Hannaske, C. Krellner, Yu. Kucherenko, M. Shi, M. Radovic, E. Rienks, G. Zwicknagl, K. Matho, J. W. Allen, C. Laubschat, C. Geibel, and D. V. Vyalikh, Phys. Rev. X **5**, 011028 (2015).

[56] Q. Y. Chen, D. F. Xu, X. H. Niu, R. Peng, H. C. Xu, C. H. P. Wen, X. Liu, L. Shu, S. Y. Tan, X. C. Lai, Y. J. Zhang, H. Lee, V. N. Strocov, F. Bisti, P. Dudin, J.-X. Zhu, H. Q. Yuan, S. Kirchner, and D. L. Feng, Phys. Rev. Lett. **120**, 066403 (2018).

[57] M. C. Aronson, M. B. Maple, R. Chau, A. Georges, A. M. Tsvelik, and R. Osborn, J. Phys. Condens. Matter **8**, 9815 (1996).

[58] W. Montfrooij, M. C. Aronson, B. D. Rainford, J. A. Mydosh, A. P. Murani, P. Haen, and T. Fukuhara, Phys. Rev. Lett. **91**, 087202 (2003).

[59] G. M. Schmiedeshoff, E. D. Mun, A. W. Lounsbury, S. J. Tracy, E. C. Palm, S. T. Hannahs, J.-H. Park, T. P. Murphy, S. L. Bud'ko, and P. C. Canfield, Phys. Rev. B **83**, 180408 (2011).

[60] B. Coqblin and J. R. Schrieffer, Phys. Rev. **185**, 847 (1969).

# Emergent holon state with a “partially” enlarged electron Fermi surface in the Kondo-Heisenberg model

## - Supplemental Material -

Jiangfan Wang<sup>1</sup> and Yi-feng Yang<sup>1,2,3,\*</sup>

<sup>1</sup>*Beijing National Laboratory for Condensed Matter Physics,*

*Institute of Physics, Chinese Academy of Science, Beijing 100190, China*

<sup>2</sup>*School of Physical Sciences, University of Chinese Academy of Sciences, Beijing 100190, China*

<sup>3</sup>*Songshan Lake Materials Laboratory, Dongguan, Guangdong 523808, China*

### I. Self-consistent equations

We start with the action of the Schwinger boson  $\text{Sp}(N)$  Kondo-Heisenberg model,

$$\begin{aligned} S = & -\frac{1}{\beta\mathcal{V}} \sum_{\mathbf{p}m\alpha a} c_{\mathbf{p}m\alpha a}^* (i\omega_m - \varepsilon_{\mathbf{p}}) c_{\mathbf{p}m\alpha a} - \frac{1}{\beta\mathcal{V}} \sum_{\mathbf{p}n\alpha} b_{\mathbf{p}n\alpha}^* (i\nu_n - \lambda) b_{\mathbf{p}n\alpha} \\ & + \frac{1}{(\beta\mathcal{V})^2\sqrt{N}} \sum_{\mathbf{p}\mathbf{k}mn\alpha a} (b_{\mathbf{p}n\alpha}^* c_{\mathbf{k}m\alpha a} \chi_{\mathbf{p}-\mathbf{k}, n-m-1, a} + h.c.) + \frac{1}{\beta\mathcal{V}} \sum_{\mathbf{p}m\alpha} \frac{|\chi_{\mathbf{p}m\alpha}|^2}{J_K} \\ & - \frac{1}{\beta\mathcal{V}} \sum_{\mathbf{p}n\alpha} (i\Delta^* \tilde{\alpha} b_{\mathbf{p}n\alpha} b_{-\mathbf{p}, -n, -\alpha} \xi_{\mathbf{p}} + h.c.) + N\beta\mathcal{V} \left( 2|\Delta|^2/J_H - \lambda\kappa \right), \end{aligned} \quad (\text{S1})$$

from which the spinon and holon Green’s functions can be derived using the Luttinger-Ward functional or the Dyson-Schwinger equations,

$$G_b(\mathbf{p}, i\nu_n) \equiv -\frac{1}{\beta\mathcal{V}} \langle b_{\mathbf{p}n\alpha} b_{\mathbf{p}n\alpha}^* \rangle = \frac{-\gamma_b(-\mathbf{p}, -i\nu_n)}{4|\Delta|^2 \xi_{\mathbf{p}}^2 - \gamma_b(\mathbf{p}, i\nu_n) \gamma_b(-\mathbf{p}, -i\nu_n)}, \quad (\text{S2})$$

$$G_{\chi}(\mathbf{p}, i\omega_m) \equiv -\frac{1}{\beta\mathcal{V}} \langle \chi_{\mathbf{p}m\alpha} \chi_{\mathbf{p}m\alpha}^* \rangle = \frac{1}{-1/J_K - \Sigma_{\chi}(\mathbf{p}, i\omega_m)}, \quad (\text{S3})$$

where  $\xi_{\mathbf{p}} = \sin p_x + \sin p_y$  comes from the Fourier transform of the spinon pairing term, and  $\gamma_b(\mathbf{p}, i\nu_n) \equiv i\nu_n - \lambda - \Sigma_b(\mathbf{p}, i\nu_n)$  is the inverse spinon Green’s function at  $\Delta = 0$ . The self-energies depend self-consistently on the Green’s functions as

$$\Sigma_b(\mathbf{p}, i\nu_n) = -\frac{\kappa}{\beta\mathcal{V}} \sum_{\mathbf{k}m} g_c(\mathbf{p} - \mathbf{k}, i\nu_n - i\omega_m) G_{\chi}(\mathbf{k}, i\omega_m), \quad (\text{S4})$$

$$\Sigma_{\chi}(\mathbf{p}, i\omega_m) = \frac{1}{\beta\mathcal{V}} \sum_{\mathbf{k}n} g_c(\mathbf{k} - \mathbf{p}, i\nu_n - i\omega_m) G_b(\mathbf{k}, i\nu_n), \quad (\text{S5})$$

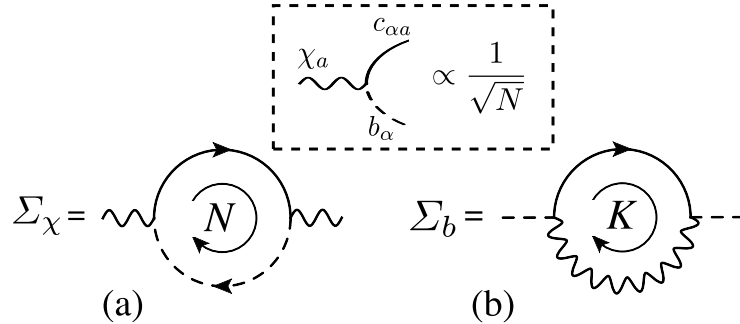


FIG. S1: The leading order skeleton diagram of (a)  $\Sigma_{\chi}$  and (b)  $\Sigma_b$ . Circles denote summation over  $N$  spin or  $K$  channel indices, which cancel the  $1/N$  factor from the two vertices. The bare three-point vertex is shown on top and proportional to  $1/\sqrt{N}$ .

with  $g_c(\mathbf{k}, i\omega_m) = [i\omega_m + (\cos k_x + \cos k_y)/2]^{-1}$  being the bare Green's function of conduction electrons. The structure of the self-energies can be illustrated via the skeleton Feynman diagrams in Fig. S1. There are no vertex corrections and conduction electron self-energy in the large- $N$  limit.

The variational parameters  $\lambda$  and  $\Delta$  can be determined via

$$\frac{\partial \ln Z}{\partial \lambda} = \frac{\partial \ln Z}{\partial \Delta} = 0, \quad (\text{S6})$$

where  $Z = \int_{[c, b, \chi]} \exp[-S]$  is the partition function of Eq. (S1). These lead to the following constraints:

$$\kappa = -\frac{1}{\beta \mathcal{V}} \sum_{\mathbf{p}n} G_b(\mathbf{p}, i\nu_n), \quad (\text{S7})$$

$$\frac{1}{J_H} \left( 1 + \frac{12\zeta|\Delta|^2}{J_H^2} \right) = -\frac{1}{\beta \mathcal{V}} \sum_{\mathbf{p}n} \frac{\xi_{\mathbf{p}}^2}{4|\Delta|^2 \xi_{\mathbf{p}}^2 - \gamma_b(\mathbf{p}, i\nu_n) \gamma_b(-\mathbf{p}, -i\nu_n)}, \quad (\text{S8})$$

where  $12\zeta|\Delta|^2/J_H^2$  comes from the biquadratic term,  $-\zeta J_H \sum_{\langle ij \rangle} (S_i \cdot S_j)^2$ , which is introduced to remedy artificial first-order transitions in the Schwinger boson mean-field theory. In the physical SU(2) case, it can be absorbed into the quadratic exchange term,

$$H_H = J_H \sum_{\langle ij \rangle} \left( S_i \cdot S_j - \zeta (S_i \cdot S_j)^2 \right) = \left( 1 + \frac{\zeta}{2} \right) J_H \sum_{\langle ij \rangle} S_i \cdot S_j + C, \quad (\text{S9})$$

where  $C$  is a constant. In the large- $N$  limit, both terms can be factorized using the mean-field variable  $\Delta_{ij}$ :

$$-\frac{J_H}{N} \sum_{\langle ij \rangle} B_{ij}^\dagger B_{ij} \rightarrow \sum_{\langle ij \rangle} \left( \frac{N}{J_H} |\Delta_{ij}|^2 + B_{ij}^\dagger \Delta_{ij} + \Delta_{ij}^* B_{ij} \right), \quad (\text{S10})$$

$$\frac{2J'_H}{N^3} \sum_{\langle ij \rangle} (B_{ij}^\dagger B_{ij})^2 \rightarrow \sum_{\langle ij \rangle} \left( -\frac{6N J'_H}{J_H^4} |\Delta_{ij}|^4 - \frac{4J'_H}{J_H^3} |\Delta_{ij}|^2 (B_{ij}^\dagger \Delta_{ij} + \Delta_{ij}^* B_{ij}) \right), \quad (\text{S11})$$

where  $B_{ij} \equiv \sum_{\alpha} \tilde{a} b_{i\alpha} b_{j,-\alpha}$ , and  $J'_H = -\zeta J_H$  has been scaled to  $(2/N)^3 J'_H$  in order for a mean-field expansion in terms of  $1/N$ . The second term on the right hand side of Eq. (S11) can be ignored for  $-4J'_H|\Delta_{ij}|^2/J_H^3 \ll 1$ . In our case, a small  $\zeta \approx 0.33$  is enough to get rid of all artificial first-order transitions. We find  $-4J'_H|\Delta_{ij}|^2/J_H^3 \sim 10^{-2}$  near the AFM QCP.

## II. Two limits: $\kappa = 0$ and $J_K = 0$

Based on Eq. (S4) and the fact  $G_\chi = 0$  at  $J_K = 0$ , it is evident that the spinon self-energy vanishes in both limits. The constraints are then simplified to

$$\kappa = \frac{1}{2\mathcal{V}} \sum_{\mathbf{p}} \frac{\lambda}{\epsilon_{\mathbf{p}}} \coth \left( \frac{\beta \epsilon_{\mathbf{p}}}{2} \right) - \frac{1}{2}, \quad (\text{S12})$$

$$\frac{1}{J_H} = \frac{1}{2\mathcal{V}} \sum_{\mathbf{p}} \frac{\xi_{\mathbf{p}}^2}{\epsilon_{\mathbf{p}}} \coth \left( \frac{\beta \epsilon_{\mathbf{p}}}{2} \right), \quad (\text{S13})$$

where  $\epsilon_{\mathbf{p}} = \sqrt{\lambda^2 - 4|\Delta|^2 \xi_{\mathbf{p}}^2}$  is the dispersion of free spinons.

For  $\kappa = 0$  and zero temperature ( $\beta = \infty$ ), the above equations require  $\Delta = 0$  for any finite  $J_H$ , which implies completely local and independent spinons. We have thus the single impurity Kondo effect in the  $\kappa = 0$  limit. To show the Fermi surface jump, we note that, because  $G_b$  is momentum independent in this limit, the holon self-energy also becomes momentum independent and reduces to

$$\Sigma_\chi(i\omega_m) = \frac{1}{\beta} \sum_n g_c(i\nu_n - i\omega_m) G_b(i\nu_n), \quad (\text{S14})$$

where  $g_c(i\omega_m) = \frac{1}{\mathcal{V}} \sum_{\mathbf{k}} g_c(\mathbf{k}, i\omega_m)$  is the momentum averaged conduction electron Green's function. At zero temperature, the real part of holon self-energy at the Fermi energy can be calculated as

$$\Sigma'_\chi(0) = - \int_{-\infty}^0 \frac{dz}{\pi} \frac{g_c''(z)}{z - \lambda}, \quad (\text{S15})$$

which gives rise to a holon Fermi surface jump at some critical value  $\lambda = \lambda_c$  satisfying

$$V_{FS}^\chi = \frac{1}{\mathcal{V}} \sum_{\mathbf{k}} \theta(-J_K^{-1} - \Sigma'_\chi(0)) = \begin{cases} 1, & \lambda < \lambda_c \\ 0, & \lambda > \lambda_c \end{cases}. \quad (\text{S16})$$

For our model with the chosen conduction band, we find  $\lambda_c \approx 0.026$ , in good agreement with its numerical value obtained self-consistently as we approach  $\kappa = 0$  along the HFL boundary.

To see the AFM phase transition in the  $J_K = 0$  limit, we first introduce the fictitious ‘‘density of states’’,

$$\rho_0(z) \equiv \frac{1}{\mathcal{V}} \sum_{\mathbf{p}} \delta(z - \xi_{\mathbf{p}}^2) = -\frac{2}{\pi^2} \text{Im} \left\{ \frac{1}{z + i0^+} E_K \left( \frac{4}{z + i0^+} \right) \right\}, \quad (\text{S17})$$

where  $E_K(y) = \int_0^{\pi/2} dx / \sqrt{1 - y \sin^2 x}$  is the elliptic integral of the first kind. The constraints become

$$2\kappa + 1 = \int_0^4 dz \rho_0(z) \frac{\lambda}{\sqrt{\lambda^2 - 4|\Delta|^2 z}} \coth \left( \frac{\beta\sqrt{\lambda^2 - 4|\Delta|^2 z}}{2} \right), \quad (\text{S18})$$

$$\frac{2}{J_H} = \int_0^4 dz \rho_0(z) \frac{z}{\sqrt{\lambda^2 - 4|\Delta|^2 z}} \coth \left( \frac{\beta\sqrt{\lambda^2 - 4|\Delta|^2 z}}{2} \right). \quad (\text{S19})$$

Defining  $Y \equiv 4|\Delta|^2/\lambda^2$ , Eq. (S18) can be rewritten as

$$2\kappa + 1 = \int_0^4 dz \frac{\rho_0(z)}{\sqrt{1 - Yz}} \coth \left( \frac{\beta\lambda\sqrt{1 - Yz}}{2} \right). \quad (\text{S20})$$

At zero temperature, we have

$$2\kappa + 1 = \int_0^4 dz \frac{\rho_0(z)}{\sqrt{1 - Yz}} \leq 1.39. \quad (\text{S21})$$

Thus the constraint can only be satisfied for  $\kappa \leq 0.195$ . The critical  $\kappa_c \approx 0.195$  occurs when  $Y = 1/4$ , which implies a zero spinon gap at  $\mathbf{p} = (\pi/2, \pi/2)$ . Beyond  $\kappa_c$ , the ground state is AFM with spinon condensate.

### III. Numerical algorithm

Direct calculations of the full self-consistent equations are quite difficult. To reduce computational costs, we develop a numerical algorithm based on the fast Fourier transform (FFT) for

$$G(x, y; \omega) = \frac{1}{\mathcal{V}} \sum_{nm} G(n, m; \omega) e^{i2\pi(nx+my)/L}, \quad (\text{S22})$$

where  $\mathbf{r} = (x, y)$  and  $\mathbf{k} = 2\pi(n, m)/L$  with  $x, y, n, m = 0, 1, \dots, L-1$ . We have  $\mathcal{V} = L^2$  and  $L$  is the lattice size along one dimension (chosen to be 64 in our calculations). Equations (S4) and (S5) in the coordinate and real frequency space become

$$\Sigma_b(\mathbf{r}, \omega) = -\kappa \int \frac{dz}{\pi} [n_F(-z) g_c(\mathbf{r}, \omega - z) G_\chi''(\mathbf{r}, z) - n_F(\omega - z) g_c''(\mathbf{r}, \omega - z) G_\chi(\mathbf{r}, z)], \quad (\text{S23})$$

$$\Sigma_\chi(\mathbf{r}, \omega) = \int \frac{dz}{\pi} [n_B(z) g_c(-\mathbf{r}, z - \omega)^* G_b''(\mathbf{r}, z) - n_F(z - \omega) g_c''(-\mathbf{r}, z - \omega) G_b(\mathbf{r}, z)], \quad (\text{S24})$$

where  $n_B(z) = 1/(e^{\beta z} - 1)$  and  $n_F(z) = 1/(e^{\beta z} + 1)$  are the bosonic and fermionic distribution functions, respectively. In each iteration, we first use FFT to transform the Green's functions to the coordinate space, integrating out the above equations at each  $\mathbf{r}$ , and then transform the self-energies back to the momentum space to calculate the Green's functions. The lattice symmetry has also been taken into consideration such that the Brillouin zone is divided into eight equivalent regions to save the computation time.

#### IV. Two-particle correlation functions

The correlation functions were first calculated in imaginary time,

$$C_O(\mathbf{r}_i - \mathbf{r}_j, \tau - \tau') = -\langle O_i(\tau)O_j(\tau') \rangle_c, \quad (\text{S25})$$

from which the spectra in real frequency can be obtained via analytic continuation. The holon density-density correlation function with  $O_i(\tau) = \frac{1}{\sqrt{K}} \sum_a |\chi_{ia}(\tau)|^2$  is given by

$$C_{n_\chi}(\mathbf{p}, i\nu_n) = \frac{1}{\beta\mathcal{V}} \sum_{\mathbf{k}m} G_\chi(\mathbf{k}, i\omega_m) G_\chi(\mathbf{k} - \mathbf{p}, i\omega_m - i\nu_n) + O(1/N), \quad (\text{S26})$$

where the  $O(1/N)$  term contains four-point connected diagrams that can be ignored in the large- $N$  limit. The spin correlation function is defined with  $O_i(\tau) = \frac{1}{\sqrt{N}} \sum_\alpha \tilde{\alpha} b_{i\alpha}^\dagger(\tau) b_{i\alpha}(\tau)$ . Outside the AFM phase, it reduces to

$$C_S(\mathbf{p}, i\nu_n) = -\frac{1}{\beta\mathcal{V}} \sum_{\mathbf{k}n'} [G_b(\mathbf{k}, i\nu_{n'}) G_b(\mathbf{k} + \mathbf{p}, i\nu_{n'} + i\nu_n) - F_b(\mathbf{k}, i\nu_{n'}) \bar{F}_b(\mathbf{k} + \mathbf{p}, i\nu_{n'} + i\nu_n)] + O(1/N), \quad (\text{S27})$$

where  $F_b(\mathbf{p}, i\nu_n) = -(1/\beta\mathcal{V}) \tilde{\alpha} \langle b_{\mathbf{p}n\alpha} b_{-\mathbf{p}, -n, -\alpha} \rangle$  is the anomalous Green's function due to the finite amplitude of spinon pairing. The staggered spin susceptibility is given by  $\chi_{st} = -C_S(\mathbf{Q}, 0)$  at  $\mathbf{Q} = (\pi, \pi)$ .

#### V. Magnetic entropy

The magnetic entropy (divided by  $N$ ) has the following expression [1],

$$\begin{aligned} S = & -\frac{1}{\mathcal{V}} \sum_{\mathbf{k}} \int \frac{dz}{\pi} \left\{ \frac{dn_B}{dT} \left( \frac{1}{2} \text{Im} \ln [\gamma_b(\mathbf{k}, z) \gamma_b(-\mathbf{k}, -z)^* - 4|\Delta|^2 \xi_{\mathbf{k}}^2] + \Sigma_b''(\mathbf{k}, z) G_b''(\mathbf{k}, z) \right) \right. \\ & \left. + \kappa \frac{dn_F}{dT} \left( \text{Im} \ln [-G_\chi^{-1}(\mathbf{k}, z)] + \Sigma_\chi''(\mathbf{k}, z) G_\chi''(\mathbf{k}, z) - N \Sigma_c'(\mathbf{k}, z) g_c''(\mathbf{k}, z) \right) \right\}, \end{aligned} \quad (\text{S28})$$

where  $\Sigma_c(\mathbf{k}, i\omega_m) = \frac{1}{\beta\mathcal{V}N} \sum_{\mathbf{p}n} G_\chi(\mathbf{p} - \mathbf{k}, i\nu_n - i\omega_m) G_b(\mathbf{p}, i\nu_n)$  is the conduction electron self-energy. The free electron contribution has been excluded. The specific heat coefficient can be calculated using  $C/T = dS/dT$ .

---

\* yifeng@iphy.ac.cn

[1] P. Coleman, I. Paul, and J. Rech, Phys. Rev. B **72**, 094430 (2005).